7 Ultrasound of Congenital Cutaneous Conditions

Ximena Wortsman, Kharla Pizarro, Yamile Corredoira, Claudia Morales, and Laura Carreño

Introduction

This chapter reviews the congenital cutaneous conditions that are most commonly requested for an ultrasound examination.

These conditions are frequently seen in the pediatric population, but they can also be detected in adulthood.

For academic purposes, the entities are divided according to the origin, and representative cases highlight the main sonographic features of each condition.

X. Wortsman (✉)
Institute for Diagnostic Imaging and Research of the Skin and Soft Tissues, Santiago, RM, Chile

Department of Dermatology, Universidad de Chile, Santiago, RM, Chile

Department of Dermatology, Pontificia Universidad Catolica de Chile, Santiago, RM, Chile

K. Pizarro
Department of Pathology, Hospital San José, Santiago, Chile

Y. Corredoira
Department of Pathology, Hospital San Borja Arriaran, Central Campus Faculty of Medicine, Universidad de Chile, Santiago, Chile

C. Morales · L. Carreño
Department of Pathology, Dermopathology Section, Universidad de Chile, Santiago, Chile

Congenital Cutaneous Conditions

Vascular Origin

Congenital Hemangiomas

These hemangiomas are fully developed at birth, and they lack the glucose transporter GLUT1. In contrast, infantile hemangiomas usually grow within the first weeks after birth and are positive for GLUT1 [1–3]. More information on infantile hemangiomas is provided in the chapter dedicated to pediatric dermatology (Chap. 23).

Clinically, RICH (rapidly involuting hemangioma) and PICH (partially involuting hemangioma) tend to show as single bulky erythematous or purple masses, sometimes with a central depression. On the other hand, NICH (non-involuting hemangioma) usually presents as a more flat macule, plaque or bump with a pale halo in the periphery; however, these forms of presentations may overlap in some cases [1–3].

Thus, according to the clinical behavior, there are three types of congenital hemangiomas currently considered in the International Society for the Study of Vascular Anomalies (ISSVA) classification [4]:

Rapidly Involuting (RICH)

These are thoroughly developed at birth and rapidly experience a regression phase in the following months. Usually, after 1 or 1.5 years, the size

X. Wortsman (ed.), *Textbook of Dermatologic Ultrasound*,
https://doi.org/10.1007/978-3-031-08736-3_7

of these hemangiomas will be decreased dramatically or wholly involuted. In their early phase, they can bleed or present ulceration [1–3].

On sonography, they appear mainly hypoechoic and hypervascular at birth with more prominent and tortuous venous vessels, compared to infantile hemangiomas; however, they also show arterial blood flow. They could be dermal or hypodermal or less frequently involve deeper layers. During the regression phase, they become heterogeneous and then change to hyperechoic structures. Their size and degree of vascu-

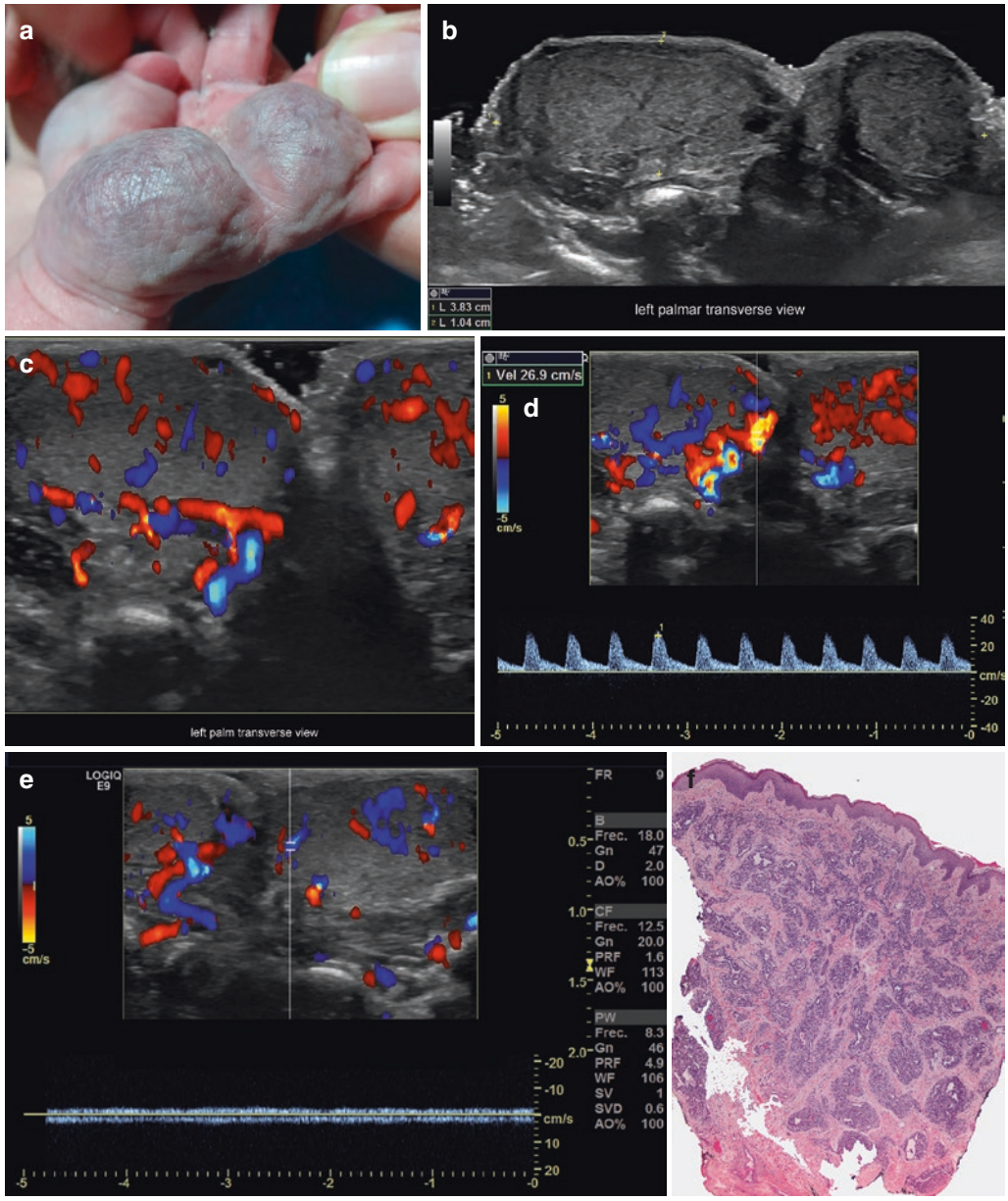

Fig. 7.1 Rapidly involuting congenital hemangioma (RICH). (**a**) Clinical lesion. (**b**) Grayscale ultrasound (transverse view) shows a hypoechoic dermal and hypodermal mass with lobulated borders. (**c**) Color Doppler demonstrates prominent vascularity within the mass. Spectral curve analyses (PW Doppler) show arterial (**d**) and venous (**e**) flow in the hemangioma. (**f**) Histology (hematoxylin and eosin (H&E) x 20): small compact and cellular lobules of collapsed capillaries in a markedly fibrotic dermis

larity decrease fast over time, and they turn to disappear; however, they may leave some residual low-flow vascularity and heterogeneous echogenicity in the tissues (Fig. 7.1) [2, 5–7].

Non-involuting (NICH)

These hemangiomas are fully developed at birth but maintain their size and features over time or slightly grow.

On ultrasound, they usually show as a heterogeneous structure, predominantly hyperechoic and with prominent vascularity. They also present arterial and venous flow and contain tortuous and dilated venous vessels. The venous vascularity is more protuberant in comparison with infantile hemangiomas. In addition, they are commonly connected to prominent subcutaneous or deeper vessels (Fig. 7.2) [2, 5–7].

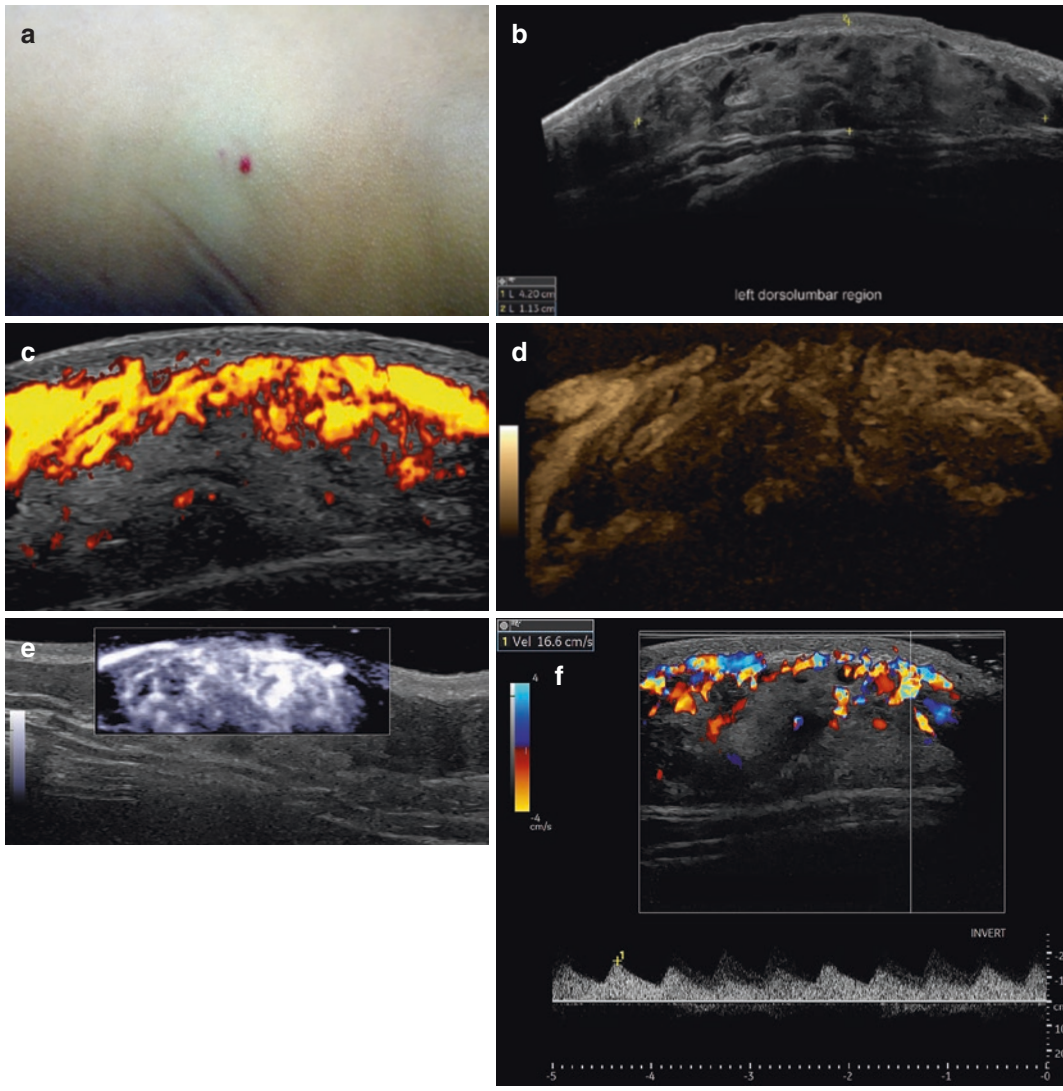

Fig. 7.2 Non-involuting congenital hemangioma (NICH). (**a**) Clinical photograph. (**b**) Grayscale ultrasound (transverse view) demonstrates heterogeneous, predominantly hyperechoic hypodermal mass with prominent, tortuous and dilated vessels. The lesion measures 4.2 cm (transverse) × 1.13 cm (thickness). (**c**, power Doppler; **d**, echoangio; **e**, microvascularity software) demonstrate the hypervascularity within the lesion. Spectral curve analyses presenting the arterial (**f**) and venous (**g**) flow in the lesion. (**h**) Histology (H&E x 20): large lobules with marked interlobular fibrosis and well-formed dilated capillary vessels are characteristic of NICH. Endothelial cells are plump and protrude into the lumina. (Courtesy of Dr. Isabel Colmenero)

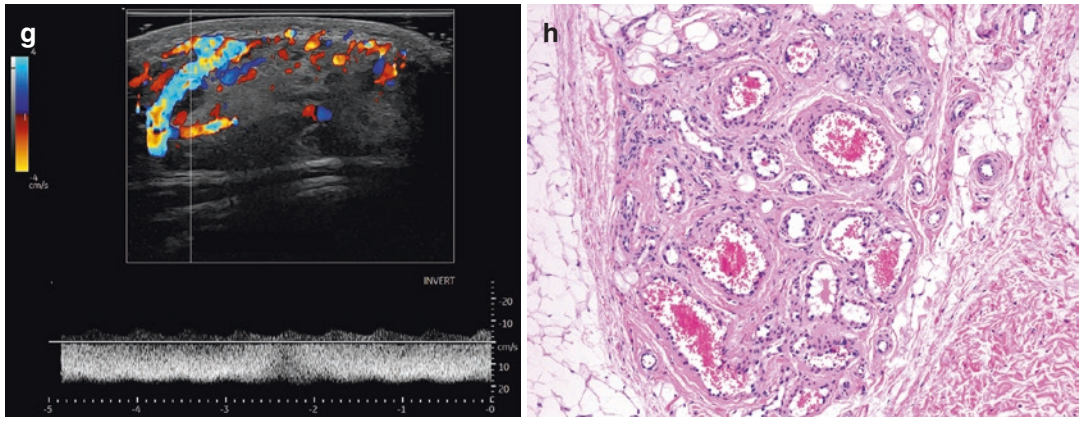

Fig. 7.2 (continued)

Partially Involuting (PICH)

These hemangiomas present an intermediate involution. They are considered an overlap of RICH and NICH hemangiomas. Clinically, they are more similar to RICH but experience a partial involution.

On ultrasound, their presentation is variable and may show signs of RICH and NICH. These hemangiomas also present prominent arterial and venous vessels with tortuous and dilated venous tracts [2, 5–7].

Other Ultrasonographic Features of Congenital Hemangiomas

Some reports mention the presence of calcifications in congenital hemangiomas [8]; however, in our experience, calcifications are much more common in low-flow venous vascular malformations [6, 7]. Additionally, some authors have explored the elastographic properties (qualitative) of congenital hemangiomas and have found a slightly lower stiffness than infantile hemangiomas [5].

Vascular Malformations (VMs)

These are errors of morphogenesis and are present at birth. These maintain their clinical features and size over time; however, they can grow in some periods of life, such as adolescence and pregnancy [6, 7, 9, 10].

VMs can be classified as arterial, venous, lymphatic, capillary, or mixed [4, 6, 7, 9, 10]. Sometimes, these types of VMs may be mixed. In addition, the VMs can appear as a single entity or may be associated with congenital syndromes [6, 7, 9, 11] (see Table 7.1).

On ultrasound, they show anechoic tubules or lacunar areas and/or focal abnormalities of the dermal and hypodermal echogenicity. These

Table 7.1 Congenital syndromes associated with vascular malformations

Syndromes	Vascular malformation
Sturge Weber	Venous
Cobb	Venous
Sacral venular	Venous
Cutis marmorata congenita	Venous
Phacomatosis pigmentovascularis	Venous
Von Hippel-Lindau	Venous
Blue rubber bleb nevus	Venous
Maffuci glomuvenous malformations	Venous and arterial
Klippel-Trenaunay	Mixed venular-venous-lymphatic
Proteus	Mixed venular-venous-lymphatic
Parkes-Weber	Mixed venular-venous-arteriovenous fistula
Rendu-Osler-Weber	Arteriovenous
Mafucci	Venous or mixed venous-lymphatic
Gorham, CLOVES	Venous and lymphatic

VMs can also involve deeper layers such as the fascia, muscles, or glands.

Phleboliths and hypoechoic endoluminal material due to thrombosis are more common in venous VM [6, 7].

Anechoic cystic lacunar areas without detectable flow are frequent in lymphatic VMs [6, 7].

The performance of spectral curve analysis is a must to distinguish between the different types of VMs [6, 7]. Therefore, at least six curves are recommended (three in longitudinal and three in transverse views) to assess the type and velocity of the blood flow within these entities [6, 7].

The arterial VMs show the typical curve in pulsed-wave Doppler with systolic and diastolic phases.

The venous VMs present the monophasic curve, and the capillary VM may show no flow because the detection threshold of the ultrasound machines does not allow it. Usually, these machines can detect blood flow with velocities ≥2 cm/s [6, 7]. In addition, Valsalva and compression/release maneuvers may facilitate the detection of venous flow [6, 7, 10].

Despite the size, lymphatic VMs commonly do not present detectable flow; however, arterial and venous flow can be detected in the periphery due to inflammation [6, 7, 10].

Mixed arterial and venous malformations frequently present shunts with the arteriovenous flow and to-and-fro curves [6, 7].

There are several types of mixed VMs, and some may gather all types of channels (Figs. 7.3, 7.4, 7.5, 7.6, and 7.7) [6, 7].

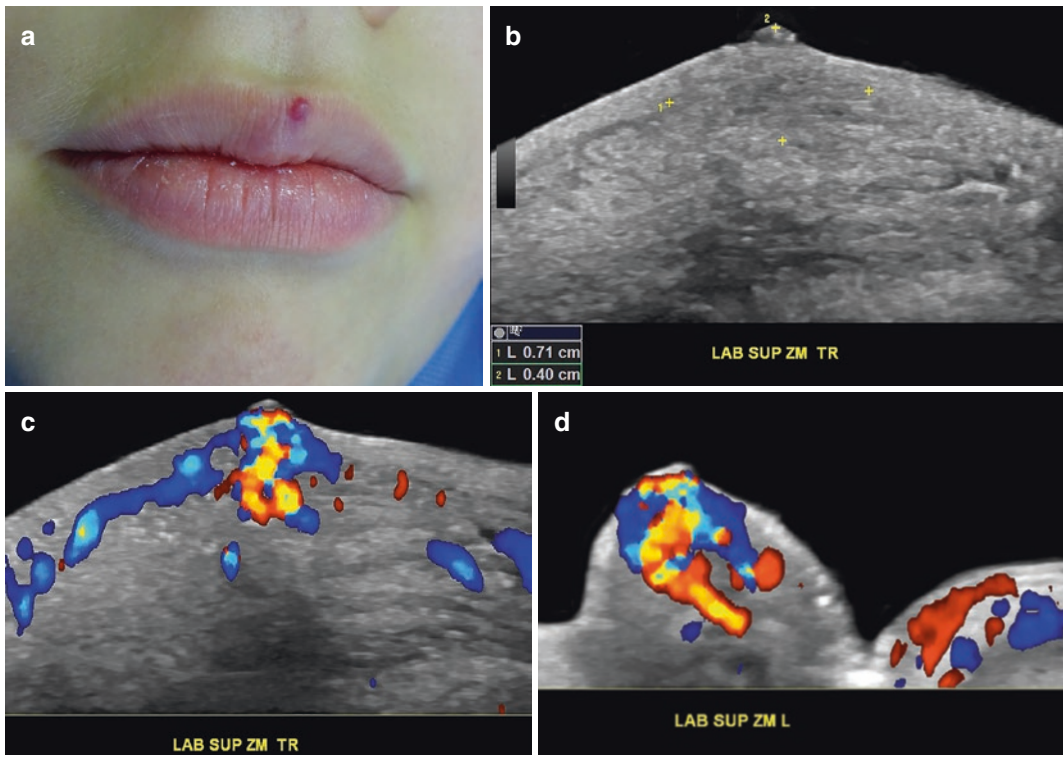

Fig. 7.3 High-flow arterial vascular malformation. (**a**) Clinical image. (**b**) Grayscale ultrasound (transverse view) shows hypoechoic dermal and muscular focal zone (within markers) in the central part of the upper lip. Color Doppler images (**c**, transverse; **d**, longitudinal) present the hypervascular nidus involving the dermis and orbicularis oris muscle of the upper lip. (**e**) Echoangio (transverse view) delineates well the vessels. (**f**) Spectral curve analysis shows arterial flow with intermediate velocity

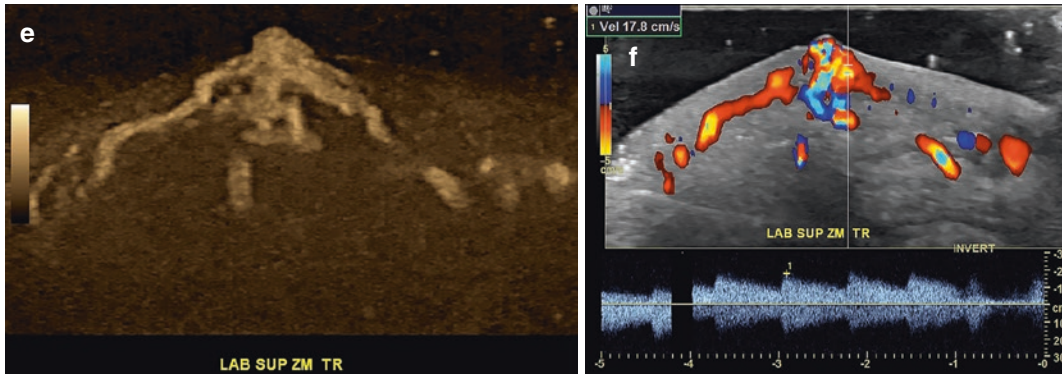

Fig. 7.3 (continued)

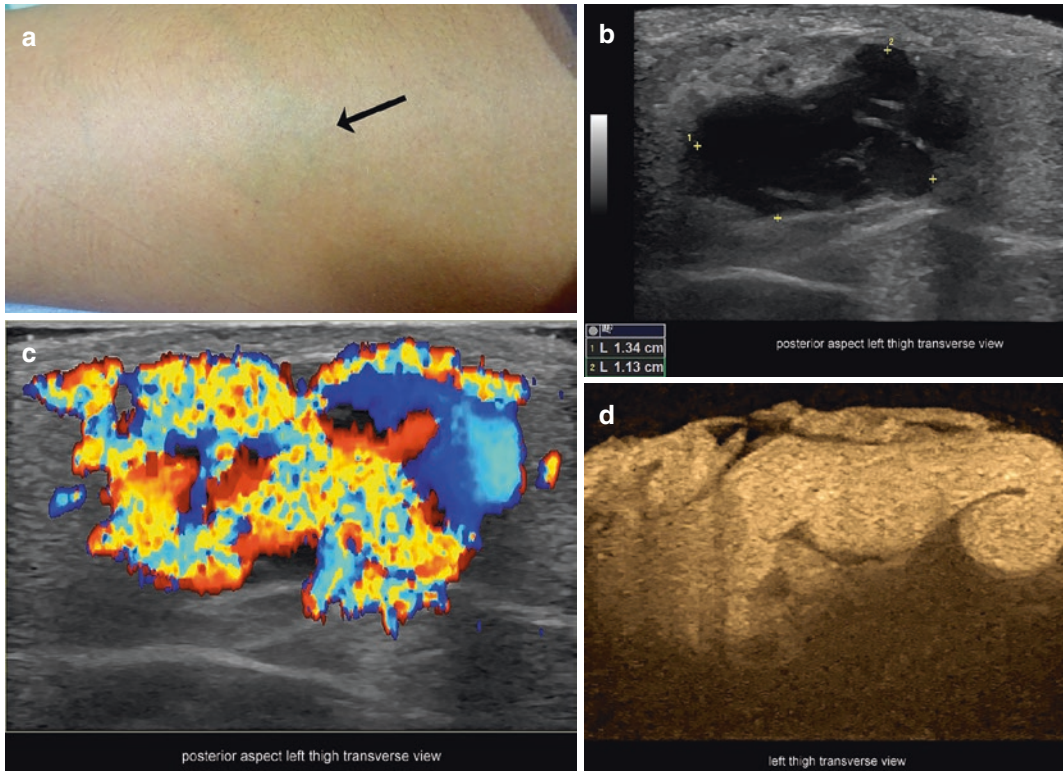

Fig. 7.4 High-flow arteriovenous vascular malformation. (**a**) Clinical photograph (arrow pointing out the lesion). (**b**) Grayscale ultrasound (transverse view posterior aspect left thigh) demonstrates anechoic lacunar hypodermal lesion. (**c**) Color Doppler and (**d**) echoangio show high hypervascularity with tortuous and dilated vessels. Notice the aliasing artifact due to the turbulent flow in the lesion. Spectral curve analyses present arterial (**e**) and venous (**f**) flow within the lesion. The peak systolic velocity is high and reaches 49.1 cm/s

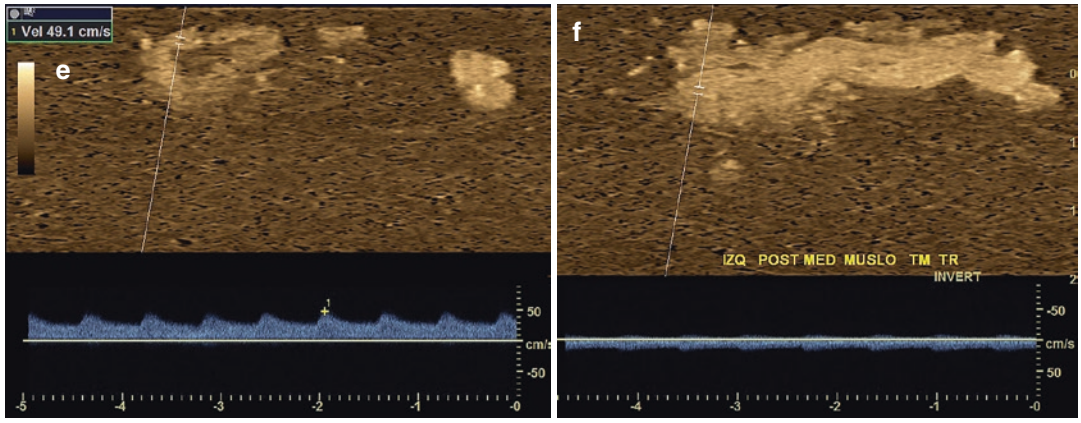

Fig. 7.4 (continued)

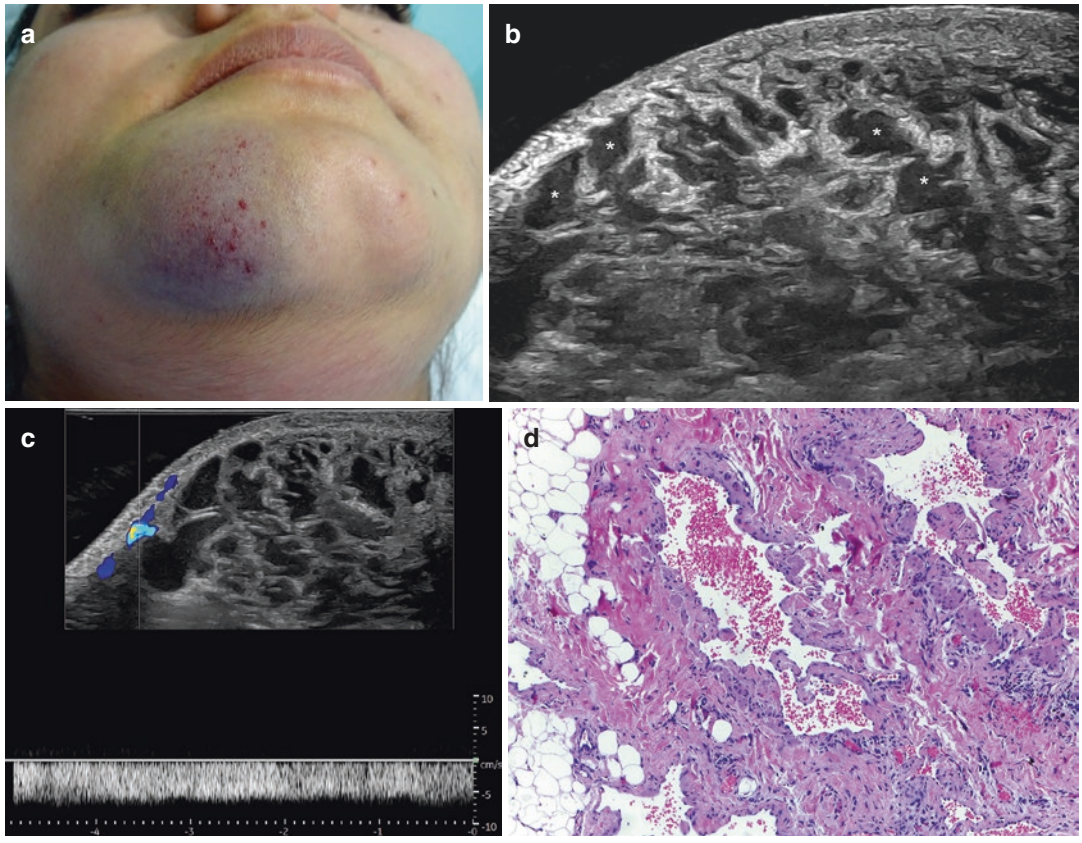

Fig. 7.5 Low-flow venous vascular malformation. (**a**) Clinical photograph. (b) Grayscale ultrasound (transverse view; right side of the chin) demonstrates multiple anechoic lacunar hypodermal spaces; some of them are marked with *). (**c**) Spectral curve analysis shows venous flow in some of the lacunar spaces and in others no presence of flow due to the low velocity within the vascular spaces (<2 cm/s). (**d**) Histology (hematoxylin and eosin × 100): dilated congested thin-walled blood vessels. Note the presence of muscle within the vessel walls

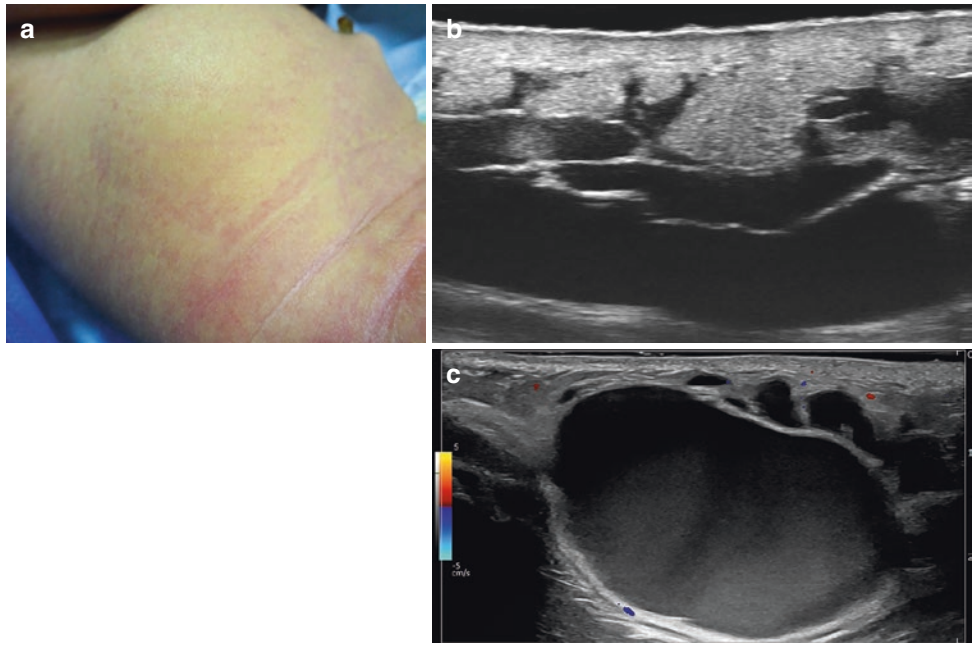

Fig. 7.6 Low-flow lymphatic vascular malformation. (**a**) Clinical picture of the right size of the abdominal wall in a 1-year-old child. (**b**) Grayscale ultrasound (70 MHz; transverse view) demonstrates multiple lacunar hypodermal spaces of different sizes and with some branches. (**c**) Color Doppler ultrasound (24 MHz) shows no presence of flow within the lacunar spaces

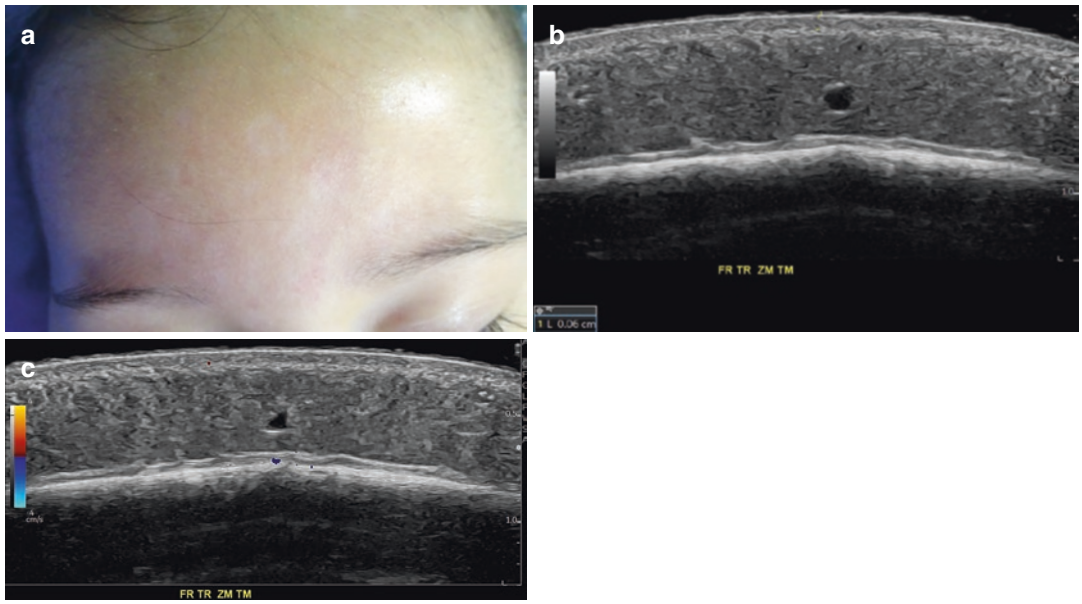

Fig. 7.7 Low-flow capillary vascular malformation. (**a**) Clinical image. (**b**) Grayscale ultrasound (transverse view) of the frontal region presents slight dermal hypoechogenicity. (**c**) Color Doppler ultrasound shows no signs of hypervascularity

Congenital Syndromes with Vascular Malformations

Several congenital syndromes present vascular malformations and are associated with the overgrowth of some corporal segments. Most of these syndromes are linked to low-flow vascular malformations; however, some present mixed vascular malformations with high- and low-flow features [11].

Of these syndromes, some correspond to the PIK3CA-related overgrowth spectrum (PROS), which is a group of rare genetic conditions that present asymmetric overgrowth caused by somatic mosaic mutations in the PI3K-AKT-mTOR pathway associated with the appearance of overgrowth. Among these, we can find CLOVES, Klippel-Trenaunay, megalencephaly-capillary malformation, dysplastic megalencephaly, fibroadipose hyperplasia or overgrowth, hemihyperplasia multiple lipomatosis, fibroadipose infiltrating lipomatosis, and some cases of macrodactyly [6, 7, 11–14].

Besides, several other congenital syndromes are associated with vascular malformations: Sturge–Weber syndrome, Proteus syndrome, blue rubber bleb nevus syndrome, Maffucci syndrome, and Osler-Weber-Rendu syndrome, among others [6, 7, 11–14].

CLOVES syndrome gathers congenital lipomatous overgrowth, vascular malformations, epidermal naevi, and skeletal and spinal anomalies such as scoliosis. In addition, a 3.3% incidence of Wilms' tumor has been reported in patients with CLOVES, which was significantly higher than in the general population (Fig. 7.8) [6, 7, 11].

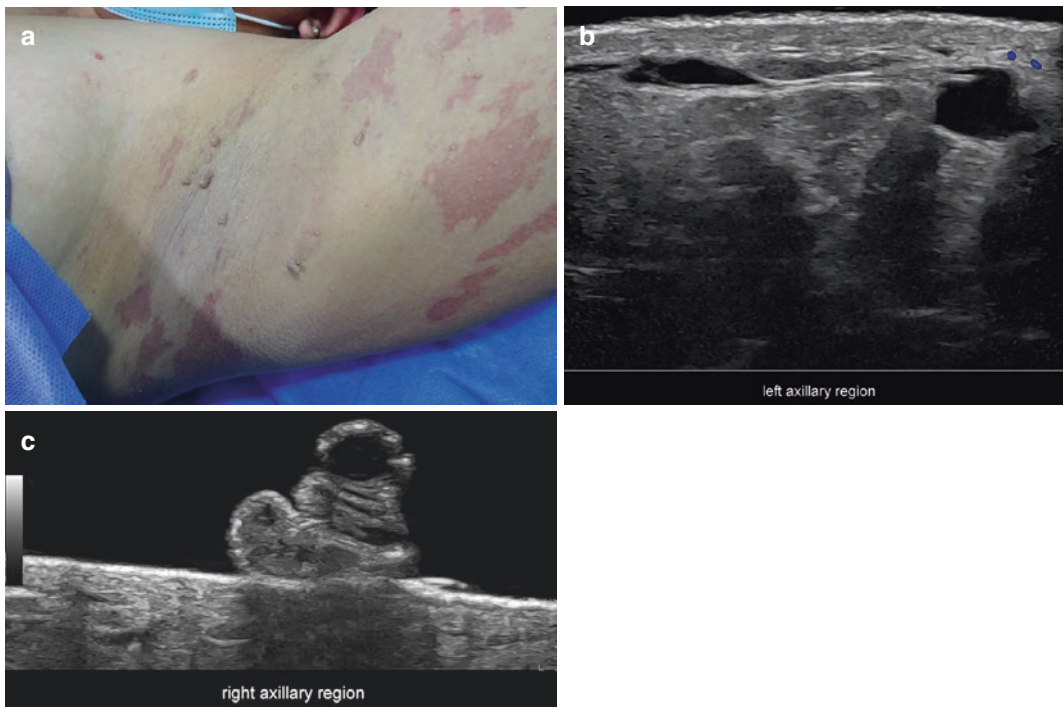

Fig. 7.8 CLOVES syndrome with low-flow venous and lymphatic vascular malformation. (**a**) Clinical picture of the left axillary region. (**b**) Color Doppler ultrasound (transverse view; left axillary region) presents lacunar anechoic hypodermal areas and some venous vessels with low-velocity venous blood flow (in blue color). (**c**) Grayscale (right axillary region) shows anechoic and hypoechoic exophytic epidermal and dermal structure compatible with lymphatic malformation

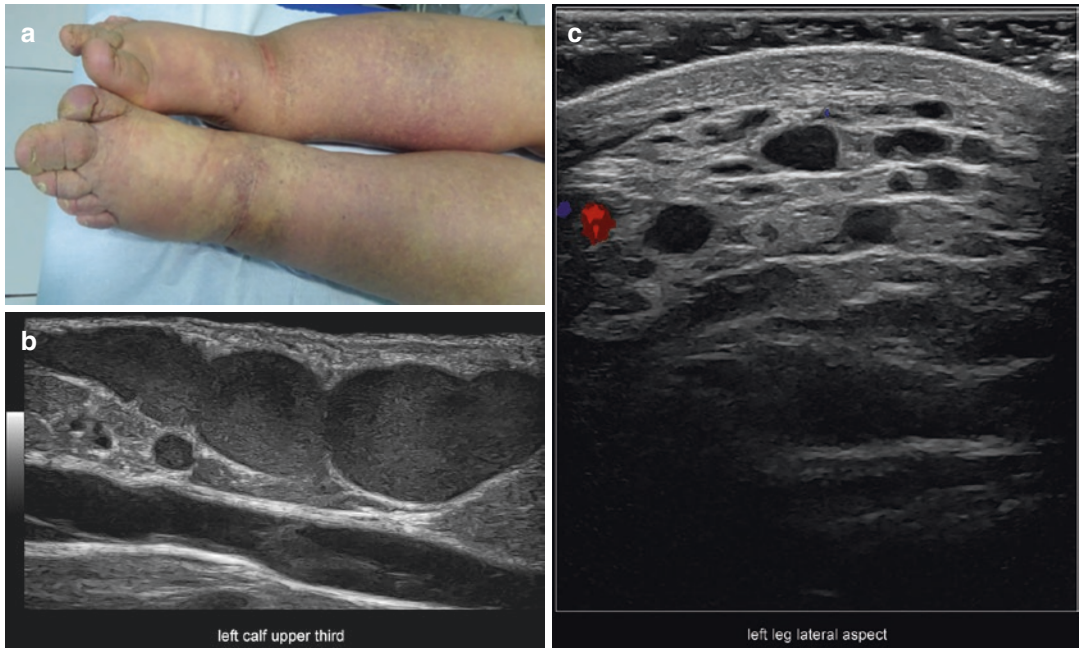

Fig. 7.9 Klippel-Trenaunay syndrome. (**a**) Clinical image. (**b**) Grayscale ultrasound (longitudinal view; left upper third of the calf) demonstrates several dilated and tortuous hypodermal veins. (**c**) Color Doppler ultrasound (transverse view; lateral aspect of the left calf) shows multiple anechoic lacunar anechoic spaces without detectable flow due to the low velocity <2 cm/s

Klippel-Trenaunay syndrome (KTS) presents asymmetric limb hypertrophy, localized capillary malformation, and congenital lower extremity varicosities. Capillary malformations are frequent in the hypertrophic limb. Limb length significant differences are usually related to underlying soft-tissue growth, long-bone hypertrophy, and lymphatic malformations. In addition, varicosities usually appear on the lateral aspect of the limb. In these cases, two open embryonic veins have been reported: the lateral marginal vein, sometimes called the vein of Servelle and the sciatic vein (Fig. 7.9) [6, 7, 11, 12, 14–16].

Parkes Weber syndrome is generated by a mutation in RASA1 and characterized by cutaneous vascular malformations [capillary, venous, lymphatic, and arteriovenous malformation (AVM)] and overgrowth. It can involve the upper or the lower extremities, including the pelvic vessels. The high-flow malformation allows us to differentiate it from KTS, in which there are only low-flow vascular malformations [6, 7, 11].

Osler-Weber-Rendu syndrome, also called hereditary hemorrhagic telangiectasia, is an autosomal dominant condition that presents arteriovenous malformations and involves the skin, mucous membranes, and internal organs. Bleeding is common in these cases and one of the first warning signs for diagnosing this condition (Fig. 7.10) [6, 7, 11].

Sturge–Weber syndrome is a neurocutaneous congenital condition that gathers facial capillary malformations (port-wine stains) and capillary-venous malformations affecting the brain and eye; however, some reports demonstrate arteriovenous malformations also associated with this entity; however, low-flow vascular malformations can also be present (Fig. 7.8) [6, 7, 11, 13].

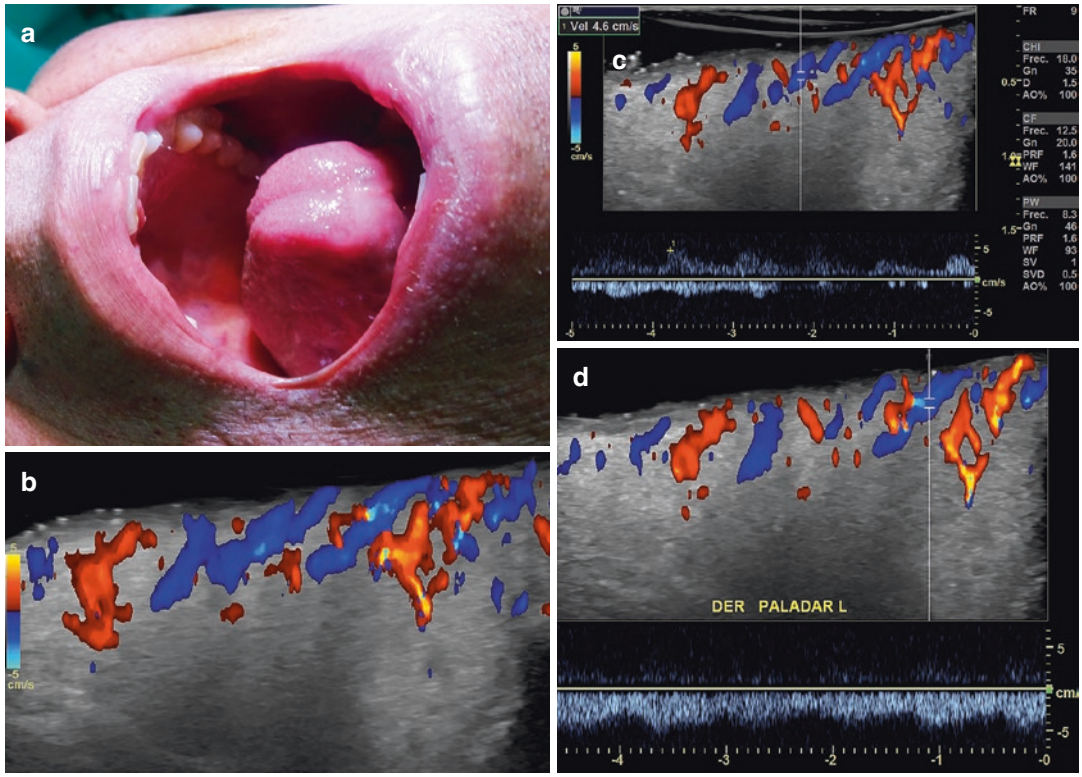

Fig. 7.10 Osler-Weber-Rendu syndrome. (**a**) Clinical image of patient with a history of multiple bleeding episodes in the oral cavity and gastrointestinal system. (**b**) Color Doppler (longitudinal view of the palate) shows submucosal hypervascularity. Spectral curve analyses demonstrate arterial (**c**) and venous (**d**) flow within the hypervascular region

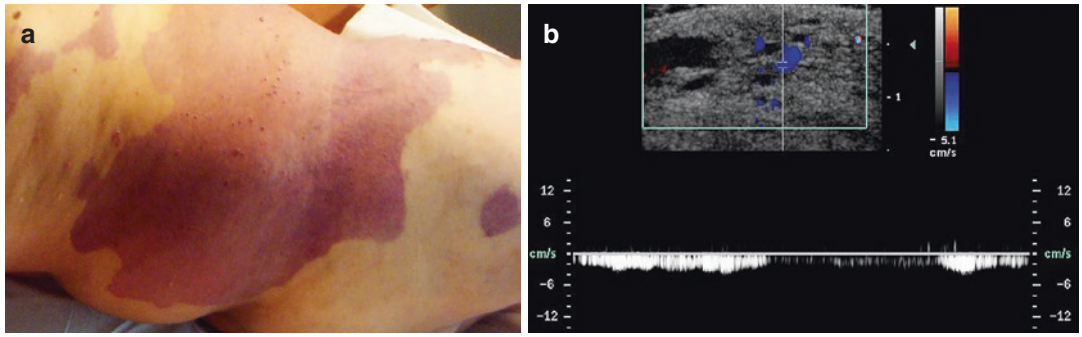

Fig. 7.11 Proteus syndrome. (**a**) Clinical image. (**b**) Color Doppler spectral curve analysis of the right side of the abdominal wall demonstrates multiple lacunar and tubular hypodermal areas showing venous flow in some of them

Proteus syndrome shows localized overgrowth, congenital lipomatosis, low-flow vascular malformations, connective tissue nevus, and epidermal nevus (Fig. 7.11) [6, 7, 11].

Maffucci syndrome presents vascular malformations and enchondromas in the distal part of the extremities [6, 7, 11].

Cysts

On ultrasound, several congenital cystic lesions can be distinguished:

Branchial Cysts or Fistulas

Also called branchial cleft cysts of fistulas, they are congenital remnants that arise from the first through fourth pharyngeal pouches. There are four branchial pouches distributed from the ear to the inferior part of the neck. These cystic or fistulous tracts commonly run through the dermis, hypodermis, and musculoaponeurotic layers. The most common are the cysts or fistulas derived from the second arch (40–95%) [6, 7, 17–22].

First branchial cysts or fistulas are subclassified through the work classification system. Work type I contains ectoderm only and presents as preauricular masses or sinuses that run anterior and medial to the external auditory canal. Work type II cysts are more common and contain both ectoderm and mesoderm. These are located at the angle of the mandible or within the submandibular region [20].

Second branchial cysts or fistulas, the most frequent ones, usually present an anterior and medial opening to the sternocleidomastoid (SCM) on the neck skin. They commonly run deep to the platysma, between the internal and external carotids, superficial to both glossopharyngeal and hypoglossal nerves, and connect to the tonsillar fossa. Usually, part of the congenital tract remains open [20].

Third branchial cysts or fistulas present an opening at the middle to the lower third of the anterior SCM. This tract runs deep to the platysma, posterior to the internal carotid artery, in between the glossopharyngeal and hypoglossal nerves, close to the superior laryngeal nerve, connecting to the pyriform sinus in the larynx [20].

Fourth branchial cysts or fistulas show an opening near the medial lower border of the SCM, and then go deep to the common carotid artery, sometimes close to the aortic arch or the subclavian vessels. Finally, they run superficial to the recurrent laryngeal nerve and hypoglossal nerve, terminating in the apex of the pyriform sinus in the larynx [20].

On histology, they are lined with stratified squamous epithelium and present keratinous debris. In some cases, the cyst wall is lined by ciliated columnar epithelium resulting in more mucoid contents. Lymphoid tissue is commonly found in the periphery of the epithelial lining [20].

On ultrasound, the cysts tend to show an oval-shaped, round-shaped, or saclike morphology, and the fistulous tracts appear as tortuous band-like structures. Their echogenicity can vary according to the degree of inflammation present in the periphery or within the cyst or fistula. Thus, they can appear as fully anechoic, hypoechoic, or mixed. On color Doppler, they may show a variable degree of vascularity in the periphery of the structure with low-flow vessels (Figs. 7.12 and 7.13) [6, 7, 18, 19, 21, 22].

Thyroglossal Cysts

Also called thyroglossal duct remnant cysts, these are remnants of a thyroid duct that connects the foramen cecum at the tongue base with the final location of the thyroid at the pretracheal inferior midline neck. It is one of the most common neck lesions with a bimodal age distribution in the first and fifth decades. There is an equal sex distribution; however, males tend to predominate in pediatric patients, while females predominate among adults. Infection and fistula formation appear in approximately 10% of cases. Three percent shows signs of malignant transformation to mostly papillary thyroid gland carcinoma [7, 10, 19, 23, 24].

Clinically, it shows as a mobile, painless midline neck mass, usually inferior to the hyoid bone. Sixty percent of them are located between the thyroid gland and the hyoid bone. The remaining 40% are found in the suprahyoid, suprasternal, and intra-lingual regions [7, 19, 22–24].

On histology, they present respiratory epithelium, squamous epithelium, or a combination of both plus inflammatory infiltrates and microscopic foci of ectopic thyroid gland tissue in the wall or its periphery [22, 25, 26].

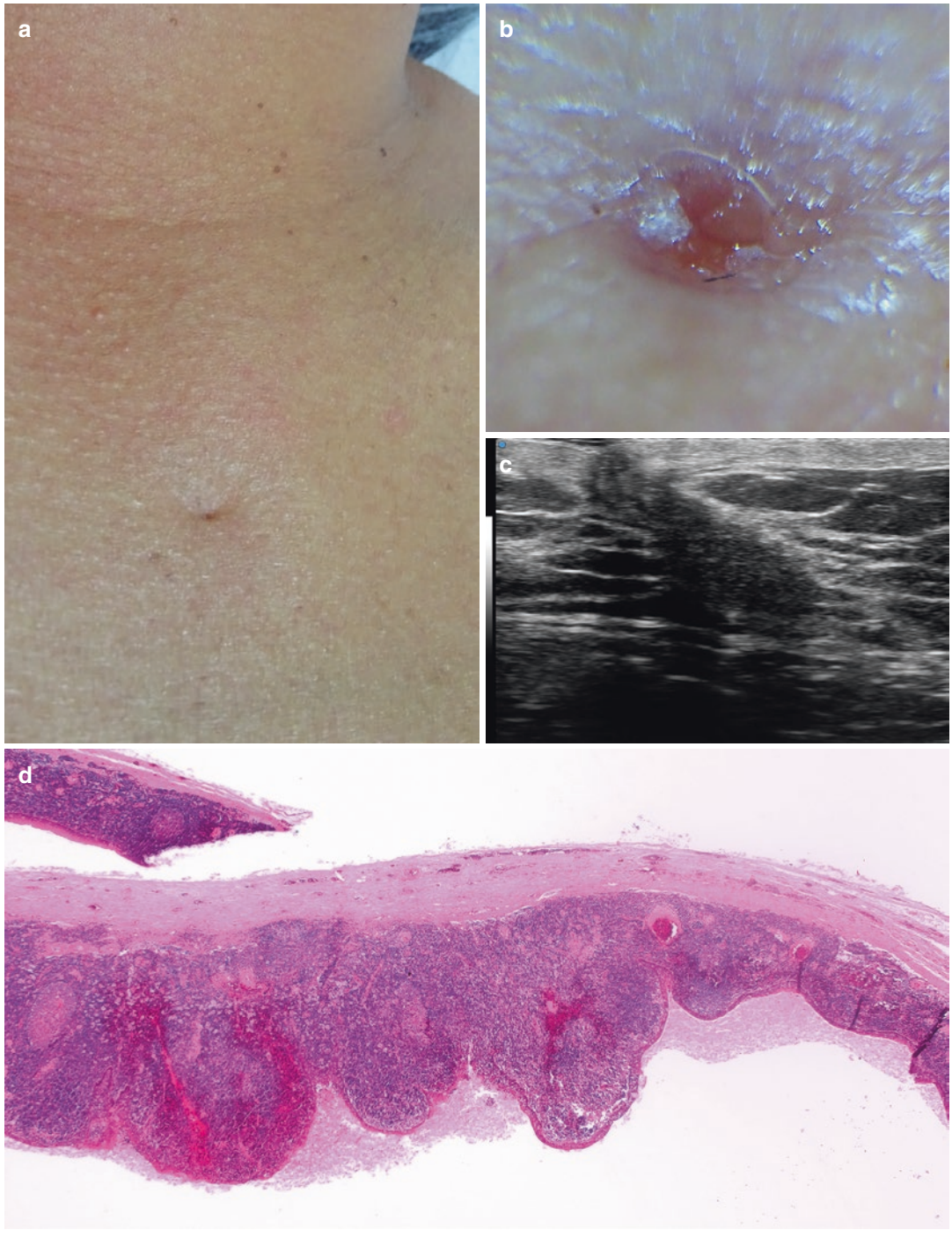

Fig. 7.12 Branchial fistula. (**a**) Clinical image. (**b**) Dermoscopy photograph. (**c**) Grayscale ultrasound demonstrates oblique hypoechoic dermal and hypodermal band. (**d**) Histology (H&E 25x): cystic lesion covered by squamous epithelium without a granular layer. There are prominent inflammatory lymphocytic infiltrates with formation of lymphoid follicles that present germinal centers

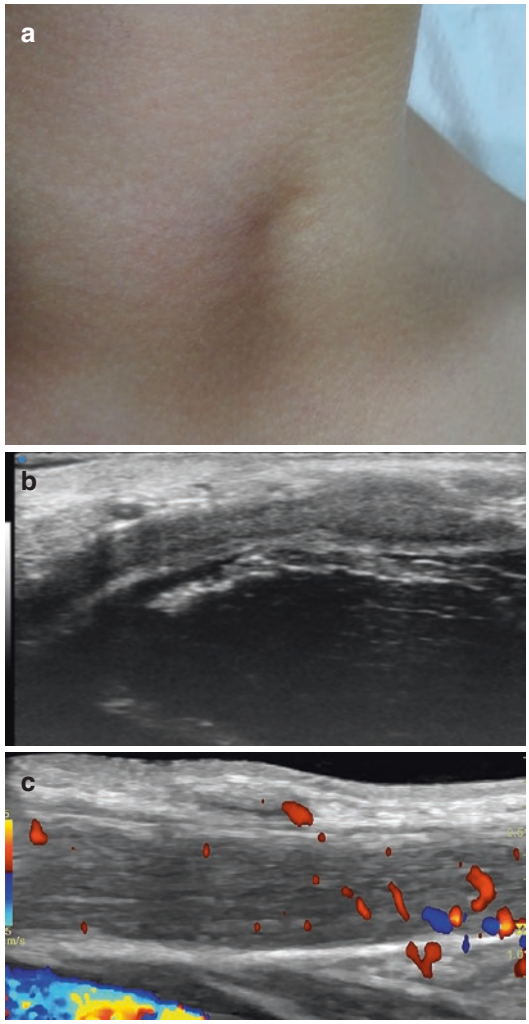

Fig. 7.13 Branchial fistula. (**a**) Clinical picture. (**b**) Grayscale ultrasound (70 MHz) shows oblique hypoechoic subaponeurotic band attached to the surface of the left sternocleidomastoid muscle. (**c**) Color Doppler ultrasound (longitudinal view; 18 MHz) demonstrates some vessels in the periphery of the fistula but no signs of vascularity within the lesion. The sternocleidomastoid muscle is located underneath the fistula and presents some vascularity.

On ultrasound, they commonly show as subcutaneous midline well-defined oval- or round-shaped, anechoic or hypoechoic cystic structures with posterior acoustic enhancement. Occasionally, floating echoes and septa may be present within the structure. The swallowing maneuver may support the finding of the synchronous movement of the tongue and the cyst. Under inflammation and infection, the wall may become irregular and the borders ill-defined. In 25% of cases, an anechoic tract is present in the cyst's periphery, commonly connecting to the underlying muscle layer [7, 10, 19, 22–25].

On color Doppler, a variable degree of vascularity may be detected in the periphery of the cyst according to the level of inflammation or the presence of secondary infection; however, usually, there is no vascularity within the cyst (Fig. 7.14) [7, 10, 19, 22–25].

The detection of hypoechoic solid tissue and hypervascularity within or in the periphery of the cyst support the presence of remnant ectopic thyroid tissue or, less likely, the development of malignant transformation [7, 10, 19, 22–25].

Dermoid Cysts

These are congenital cysts caused by aberrant ectodermal tissue sequestered in suture lines that close during embryonic development. They are typically found along the skull bone fusion lines (e.g., anterior fontanelle, lateral frontal region, tail of the eyebrow, or submandibular region). Dermoid cysts present as non-tender and firm nodules that vary in their size over time. The most common location is the eyebrow tail, but they have also been reported in the face, neck, and scalp, besides other less common locations [7, 10, 19, 24].

On ultrasound, they tend to be subaponeurotic and close to the bony margin and sutures. The most common form of presentation is the well-defined, oval-shaped, anechoic, or hypoechoic structure that commonly contains hyperechoic fragments of hair tracts, which are more evident at higher frequencies. Sometimes, hypoechoic fatty round or oval-shaped hypoechoic structures are detected within the cyst, named the "sac-of-marble" sign. Calcium deposits can also be found within dermoid cysts and show as hyperechoic deposits that move with the compression maneuver. Additionally, scalloping of the underlying bony margin may be found [7, 10, 19, 24].

On color Doppler, there are some low-flow vessels in the periphery but commonly no internal vascularity (Figs. 7.15 and 7.16) [7, 10, 24].

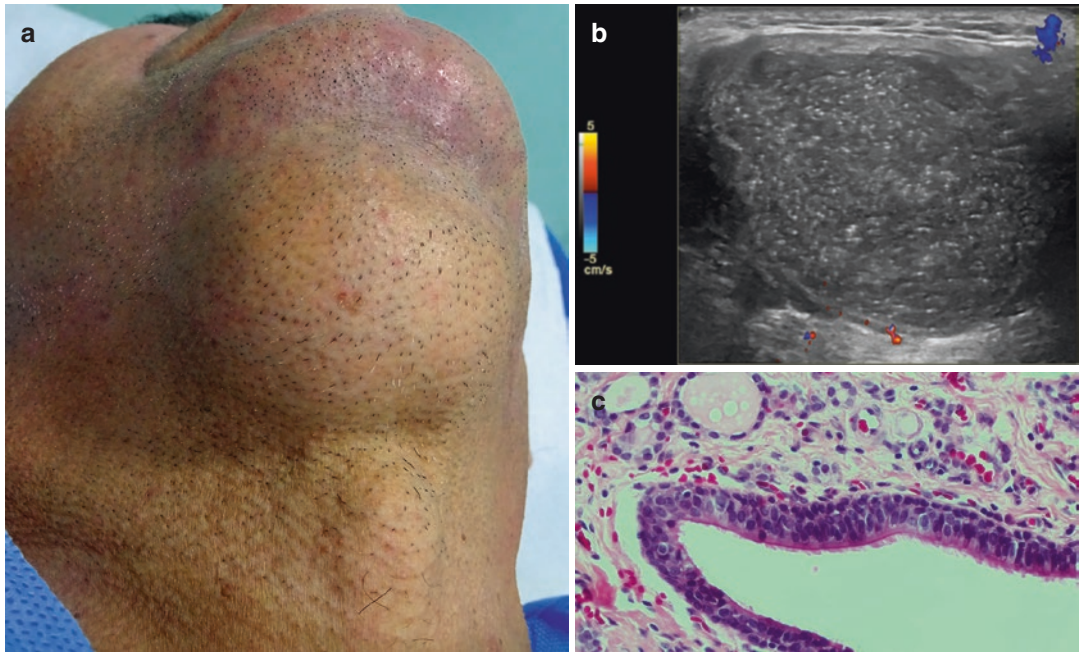

Fig. 7.14 Thyroglossal cyst. (**a**) Clinical image of the anterior neck. (**b**) Color Doppler ultrasound (transverse view; anterior neck) shows oval-shaped well-defined subaponeurotic hypoechoic structure with some bright echoes and without internal blood flow. (**c**) Histology (H&E 400x): cystic lesion covered by cylindrical ciliated pseudostratified epithelium. In the stroma, it is possible to observe thyroid follicles

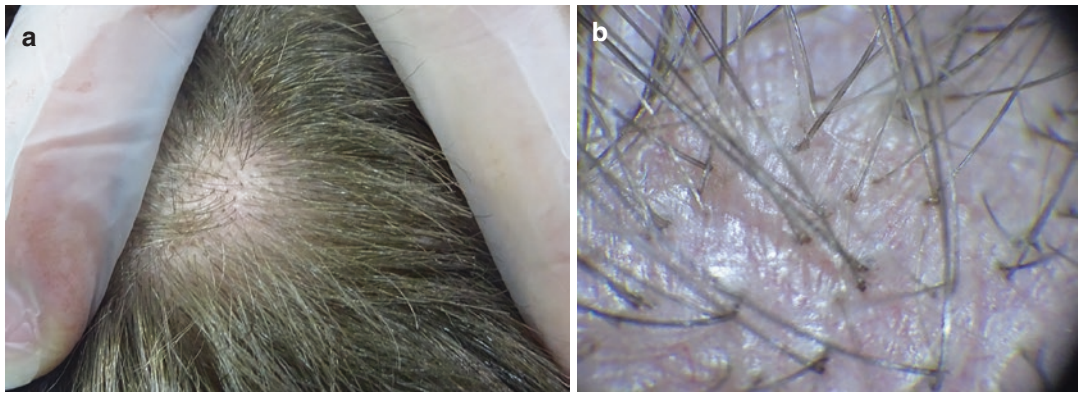

Fig. 7.15 Dermoid cyst. (**a**) Clinical photograph. (**b**) Dermoscopy image. (**c**) Grayscale ultrasound (transverse view of the scalp) presents oval-shaped, well-defined hypoechoic and anechoic subaponeurotic structure with some linear hyperechoic tracts that correspond to fragments of hair tracts. (**d**) Color Doppler ultrasound (longitudinal view) shows no vascularity within the structure and a vessel on top that corresponded to an artery. (**e**) Histology (H&E 50x): cystic lesion covered by mature squamous epithelium that produces lamellar eosinophilic keratin that presents a wall with sebaceous units and fibrotic changes

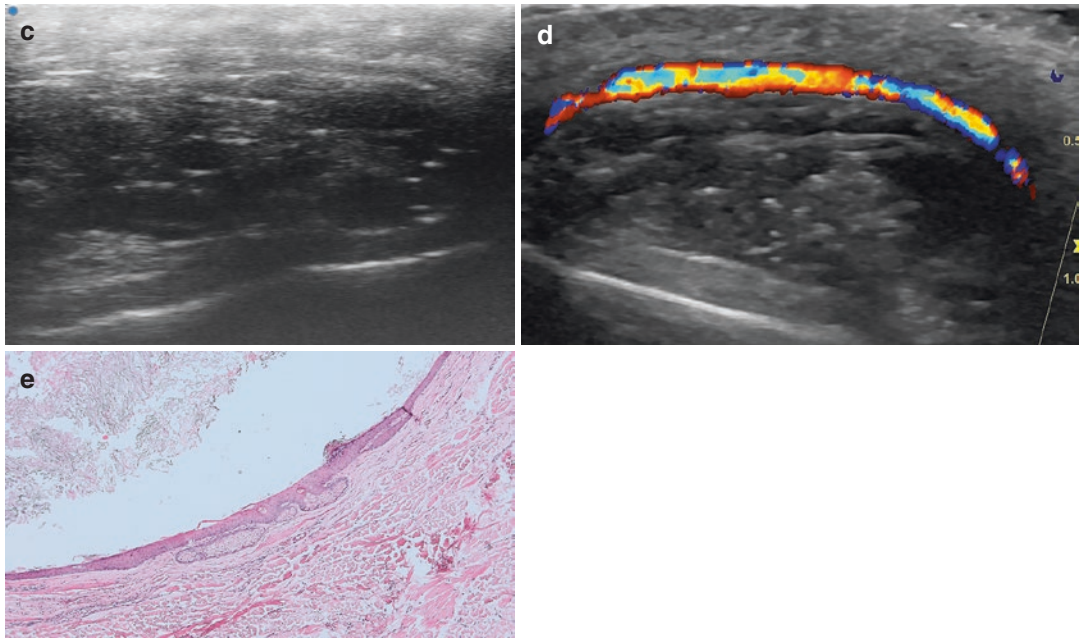

Fig. 7.15 (continued)

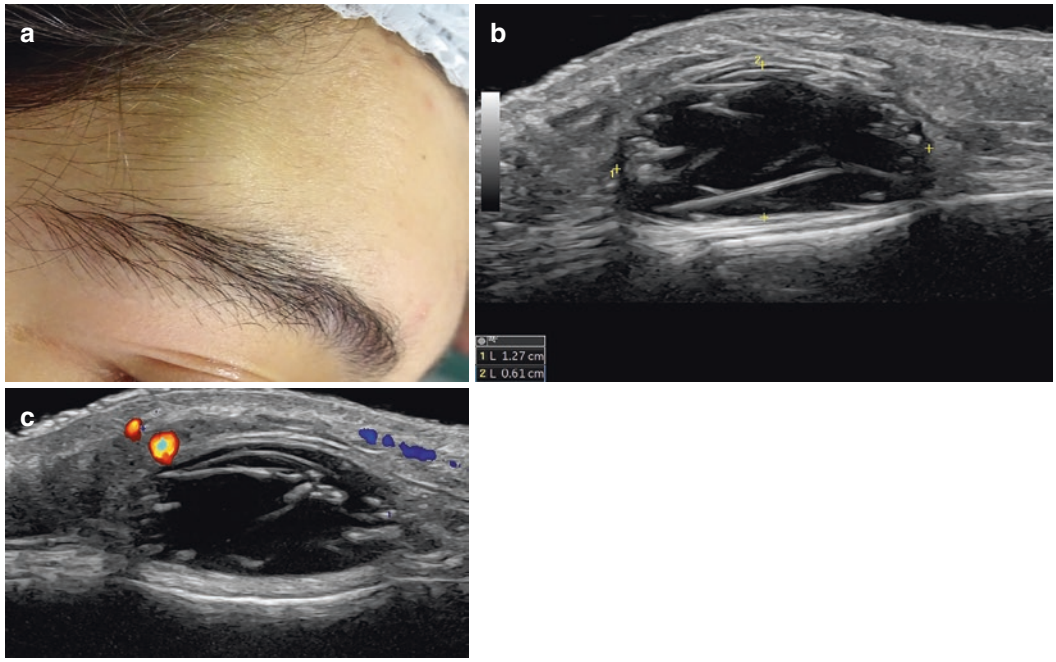

Fig. 7.16 Dermoid cyst. (**a**) Clinical lesion in the frontal region close to the tail of the eyebrow. (**b**) Grayscale ultrasound (transverse view) shows oval-shaped, well-defined subaponeurotic structure that contains hyperechoic linear bands that correspond to fragments of hair tracts. (**c**) Color Doppler ultrasound demonstrates avascularity within the mass and the frontal branch of the temporal artery (in red color) on top of the lesion

These cysts can become inflamed and increase their size and modify their inner echogenicity. The cyst rupture may also occur and generate irregularities of the walls and increase the internal and peripheral echogenicity and blood flow [24].

Auricular Pits and Fistulas (Sinuses)

These are usually located in the preauricular region at the anterior margin of the ascending limb of the helix and anterior to the external auditory canal. However, there are rare variants located in the auricular concha and the postauricular region. Auricular pits or fistulas originate from the failure of complete fusion of hillocks or entrapment of ectodermal epithelium during auricular development and contain keratinous debris. The pits are superficial and composed of dermal saclike structures. The fistulas, also called sinuses, correspond to deeper sacs or tunnels that frequently run through the dermis and hypodermis in a similar location [7, 27, 28].

Clinically, these pits and fistulas can become inflamed and infected and drain cheesy material [7, 27, 28]. Approximately 3–10% of preauricular sinuses are related to complex disorders such as deafness and branchio-oto-renal (BOR) syndrome; therefore, auditory testing and a renal ultrasound should be considered [7].

On ultrasound, the pits show as anechoic or hypoechoic dermal saclike structures. The fistulas present as anechoic or mixed anechoic and hypoechoic saclike or band-like structures. However, fistulas tend to be wider in their deep part and attach to the auricular cartilage surface (Fig. 7.17). On color Doppler, they can show variable degrees of vascularity in their periphery with low-flow arterial and/or venous vessels.

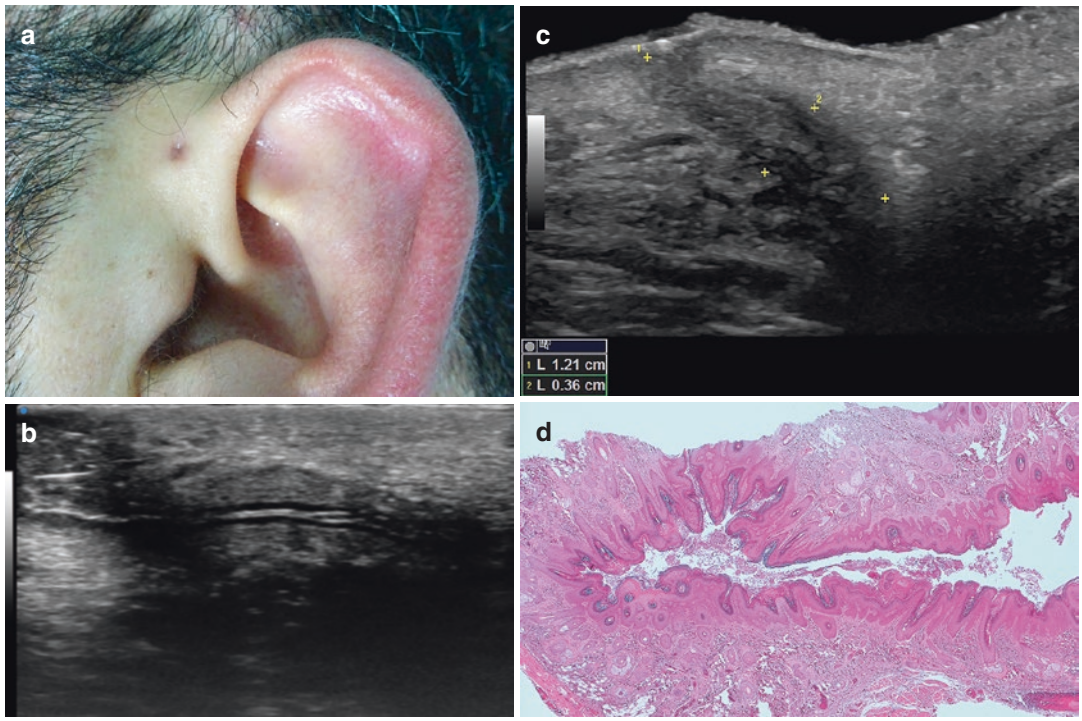

Fig. 7.17 Auricular fistula. (**a**) Clinical photograph. (**b**) Grayscale ultrasound (70 MHz; upper part of the left preauricular region) presents hypoechoic dermal band with central hyperechoic bilaminar structure. (**c**) Grayscale ultrasound (18 MHz) shows hypoechoic dermal and hypodermal oblique band located medially to the anterior auricular cartilage. (**d**) Histology (H&E 25x): cutaneous tract covered with squamous epithelium, acanthosis, hair follicles, and chronic inflammatory changes

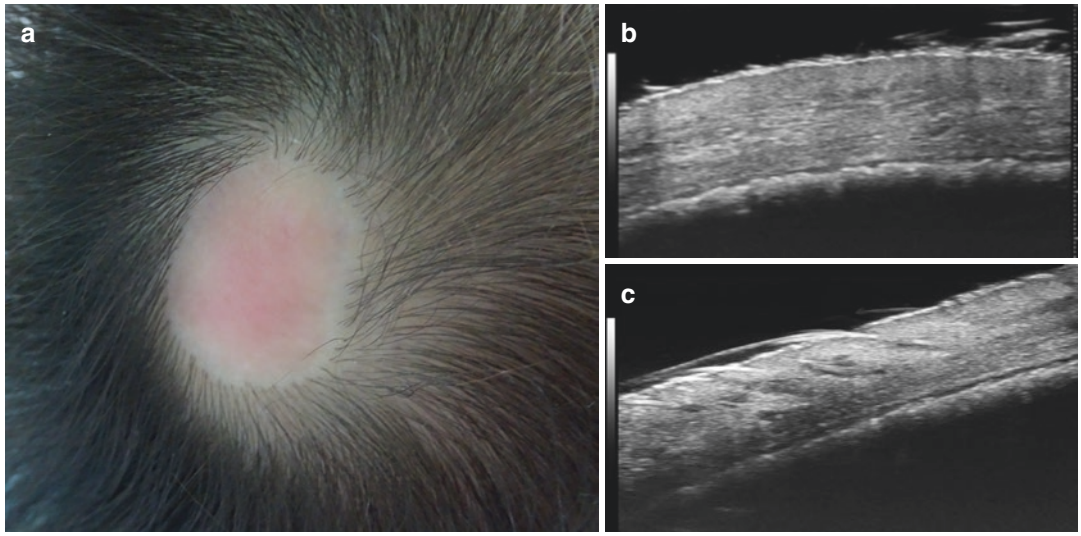

Fig. 7.18 Aplasia cutis congenita. (**a**) Clinical image. Grayscale ultrasound (70 MHz). (**b**) Notice the lack of hair follicles in the dermis and fatty tissue in the hypodermis of the lesion. (**c**) Comparative lesional (right side of the picture) versus perilesional tissue (transitional zone) highlights the difference in the presence of hair follicles between the zones

Under inflammation, the cartilage may be involved and increase its echogenicity and present hypervascularity [7, 28].

Aplasia Cutis Congenita (ACC)

It is characterized by a localized absence of skin (epidermis, dermis, or hypodermis) and has an estimated incidence of 3 per 10,000 live births. ACC may present as an isolated condition in 70% of cases or with underlying cranial and cerebrovascular defects. Eighty-six percent of ACC cases involve the scalp, most commonly the vertex region, and of these, 20–30% affect the underlying bone [29].

Clinically, it can show as ulcerations or erosions of the skin that may extend to deeper tissues, such as the muscle or bone, or may appear as an atrophic scar at birth [29].

There are two main clinical variants of scalp ACC: membranous and nonmembranous. Membranous ACC tends to present as small, oval, or round-shaped atrophic plaques with a membrane-like surface. They may or may not have a hair collar sign, where there are often longer, darker hairs in the lesion's periphery. The membranous covering may be filled with fluid or blood, giving it a bullous or bloody appearance. Hypertrophic scar-like lesions may also be seen. Nonmembranous ACC usually shows larger lesions with irregular or stellate-like erosions or ulcerations that heal with scar-like surfaces and areas with conservation of skin appendages [29, 30].

High clinical suspicion for underlying central nervous system defects should be raised in ACCs with hair collar sign, midline vertex location, size greater than 5 cm, vascular stains, and nodules. Ultrasound may support the diagnosis of CNS involvement in children aged <6 months and MRI in >6 months [29, 30].

On ultrasound, there is a lack or decrease in thickness of the epidermis, dermis, hypodermis, or deeper layers, sometimes associated with regional lack of hair follicles. On color Doppler, these lesions may show some low-flow arterial and venous vascularity (Fig. 7.18) [7].

Nevus Sebaceous of Jadassohn (NSJ)

This is a hamartomatous condition, considered an organoid nevus, that frequently appears in

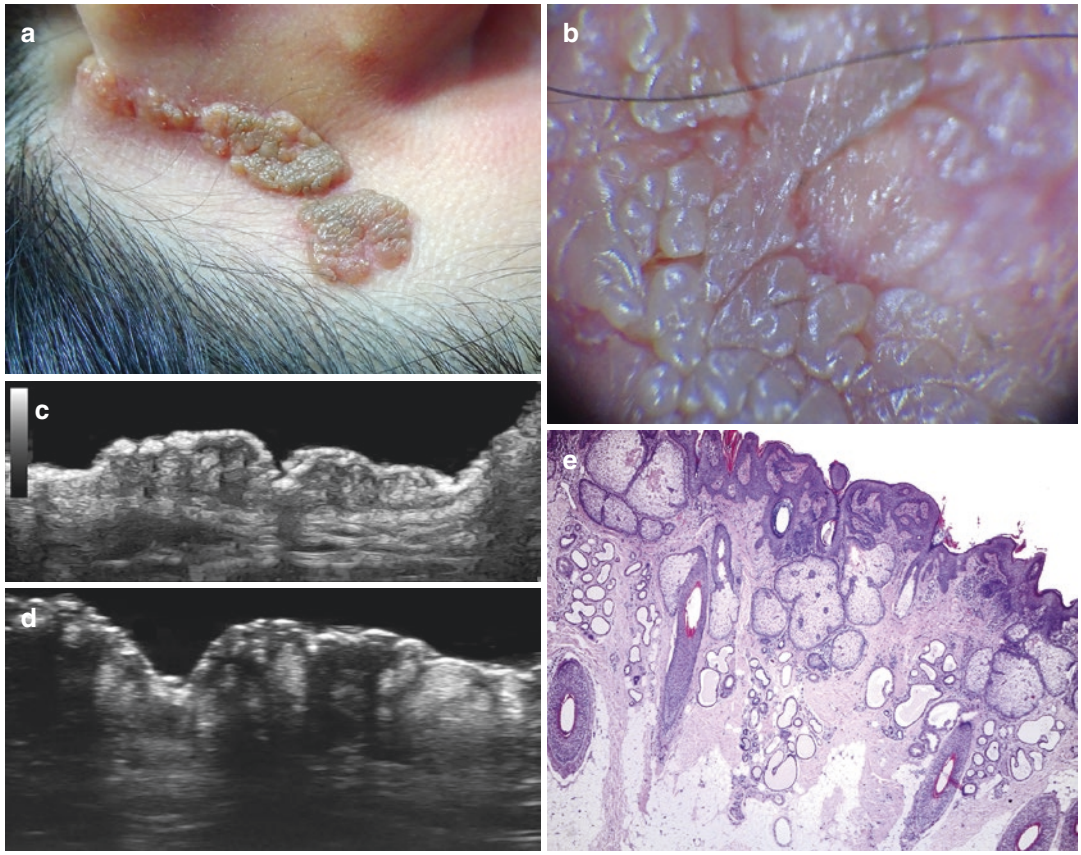

Fig. 7.19 Nevus sebaceous of Jadassohn. (**a**) Clinical image. (**b**) Dermoscopy image. Grayscale ultrasounds (**c** at 24 MHz; **d** at 70 MHz transverse view; right retroauricular region) show heterogenous dermal plaque that displaces upward the epidermis. Notice the hyperechoic oval-shaped structures within the lesion that correspond to sebaceous glands. (**e**) Histology (H&E 20x): small and distorted pilosebaceous follicles, papillomatosis, and numerous apocrine glands. Note the abnormally shaped rudimentary follicles (*)

the head of children, most commonly in the scalp; however, it may appear in other locations. It has been reported as the result of postzygotic somatic mutations of the Ras protein family [31, 32].

At birth, the lesion tends to be flat, erythematous, linear or patchy, skin-colored or yellowish plaques with hairless, orange peel-like surface. Over time, it becomes more verrucous [32]. In addition, NSJ is associated with several secondary tumors, including skin cancer that tends to appear during adulthood. Among the skin, tumors are trichoblastoma, syringocystadenoma papilliferum, basal cell carcinoma, and squamous cell carcinoma [33].

On ultrasound at 18–24 MHz, it shows as a hypoechoic or heterogeneous dermal thickening. At 70 MHz, it shows as clusters of hyperechoic oval-shaped dermal structures that correspond to sebaceous glands, some hypoechoic distorted pilosebaceous units. On color Doppler ultrasound, they present a variable degree of vascularity with low-flow vascularity (Figs. 7.19 and 7.20) [34].

Neurofibromatosis (NF)

It belongs to the phakomatoses (i.e., hereditary developmental anomalies of ectodermal tissues). It generates peripheral sheath nerve

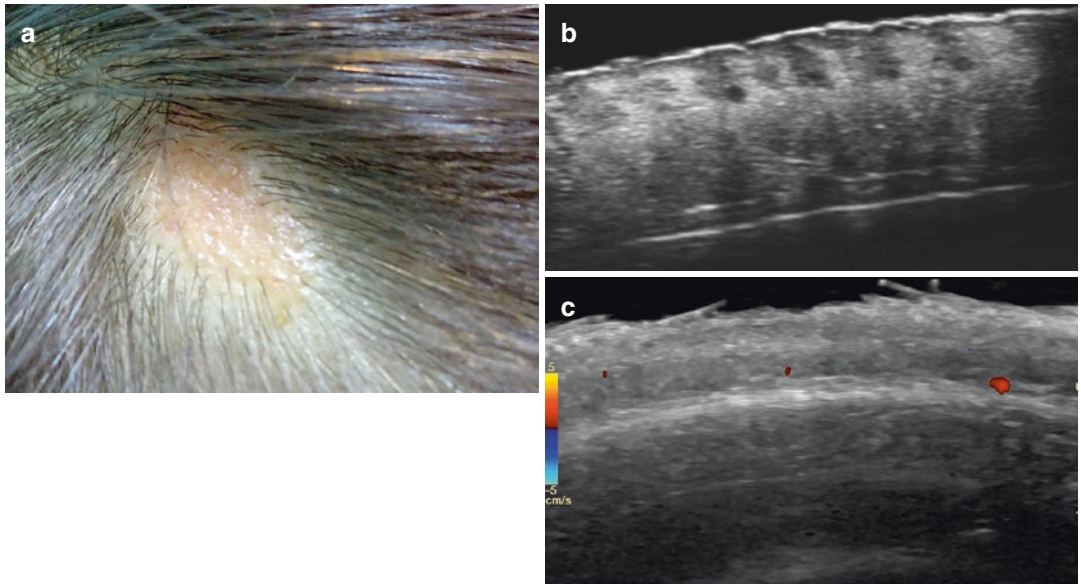

Fig. 7.20 Nevus sebaceous of Jadassohn. (**a**) Clinical picture. (**b**) Grayscale ultrasound (70 MHz; transverse view of the scalp lesion) demonstrates hypoechoic distorted pilosebaceous units in the dermis. (**c**) Color Doppler ultrasound (18 MHz; transverse view) shows no signs of hypervascularity in the lesional area

tumors that appear as hamartomas disseminated throughout the skin and deeper layers. There are at least eight different subtypes of NFs; however, NF-1 and NF-2 account for 99% of cases. NF-1 (von Recklinghausen's disease), the most common form of presentation, shows multiple café-au-lait cutaneous spots, peripheral neurofibromas, and pigmented hamartomas of the iris (Lisch nodules). NF-2 accounts for 10% of cases and affects the central nervous system presenting bilateral acoustic neurinomas, meningiomas, and spinal tumors, besides the skin involvement [7, 35, 36].

Morphologically, there are three forms of presentation of cutaneous neurofibromas: localized, plexiform, and diffuse. Localized variants, also called solitary neurofibromas, appear sonographically as oval or fusiform hypoechoic nodules. Approximately in 50% of the localized neurofibromas, it is possible to distinguish centrally located afferent and efferent neural branches that come out from the nodule. In contrast, schwannomas show eccentrically located afferent and efferent tracts [7, 35].

On color Doppler, the vascularity is variable and can range from hypovascular to hypervascular, with the hypovascular type being more frequent. Additionally, the finding of hypervascularity may be related to internal hemorrhage and inflammation. The hemorrhage within the neurofibromas appears as anechoic areas within the nodules [7].

Plexiform neurofibromas involve long nerve segments and their branches, and the tumors present a serpentine structure, also called a "bag of worms." Ultrasound shows the affected nerves and branches as multiple and tortuous hypoechoic tracts with nodular regions, commonly hypovascular on color Doppler ultrasound. The plexiform variant usually affects the hypodermal or deeper layers [7, 35, 36].

Diffuse neurofibromas present as a focal overgrowth of neural tissue. On ultrasound, they show as a focal dermal and/or hypodermal area with multiple anechoic or hypoechoic tubular and tortuous interconnected tracts and/or nodules surrounded by hyperechoic tissue, which composes a plaque-like structure. On color Doppler, the vascularity is variable and may range from hypovascular to hypervascular. However, hypovascular lesions are more common (Figs. 7.21 and 7.22) [7, 35].

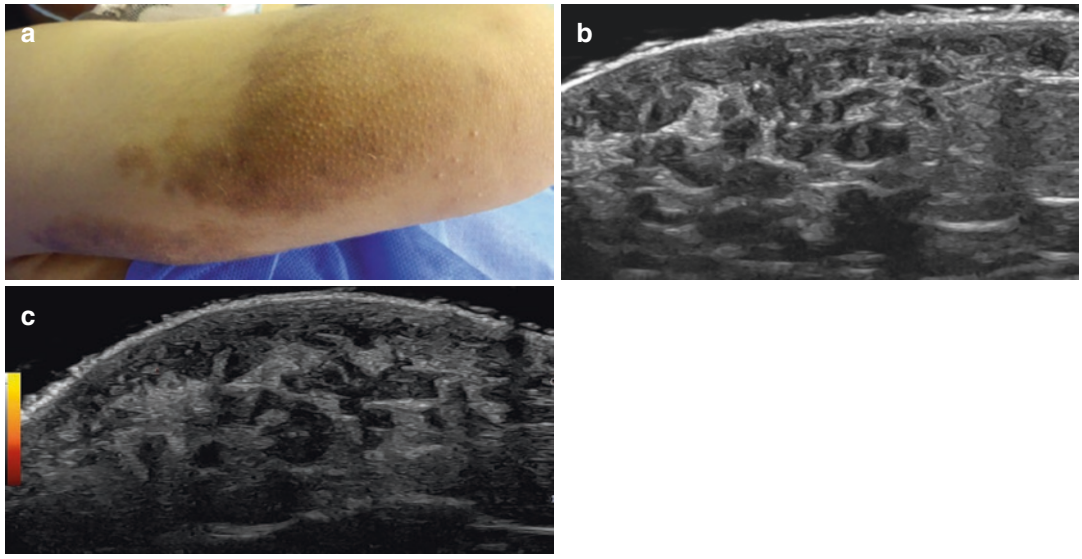

Fig. 7.21 Neurofibromatosis. (**a**) Clinical lesion. (**b**) Grayscale ultrasound (transverse view left elbow) shows multiple tortuous hypoechoic dermal and hypodermal tracts. (**c**) Power Doppler presents no signs of hypervascularity in the lesion

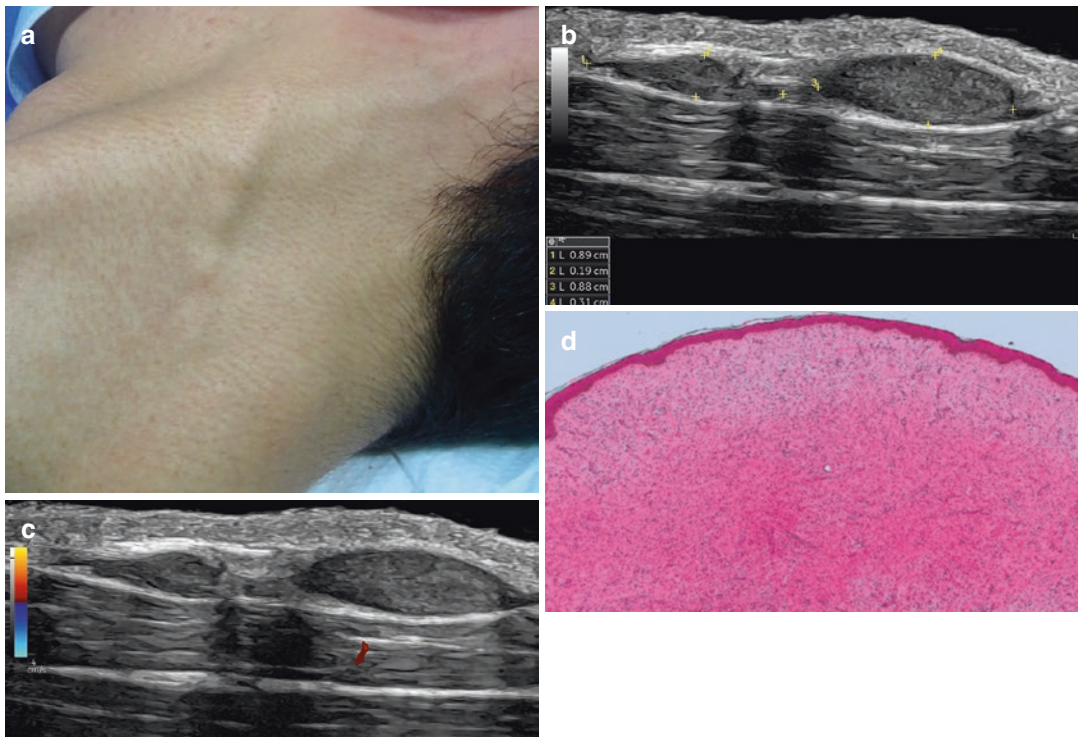

Fig. 7.22 Neurofibromatosis. (**a**) Clinical lesion with bumps on the left side of the neck. (**b**) Grayscale ultrasound (longitudinal view) of the lesional area presents two subcutaneous well-defined, oval-shaped hypoechoic nodules. These nodules are connected through a thin hypoechoic band. (**c**) Color Doppler ultrasound (longitudinal view) shows no presence of hypervascularity within the nodules. (**d**) Histology (H&E 50x): nodular dermal proliferation with fused cells that present comma-shaped nuclei and fibrillar cytoplasm without mitosis. Multiple capillary vessels and collagen bundles in the stroma, and thinning of the epidermis

On histology, NF shows a myxoid stroma, nerve cells, and fibroblasts with occasional prominent vessels. In the diffuse form of NF, atypical Schwann cells with short fusiform contours are interspersed within a uniform matrix of collagen [7].

There are also mixed forms of presentations that gather these subtypes in the same patient [7].A sudden growth or hypervascularity within the nodules may raise the suspicion for malignant transformation; however, the malignant transformation of neurofibromas is extremely rare. Among the signs of malignant transformation of NF are tumor size ≥7 cm, lobulations, heterogenicity, irregular contours, hypervascularity, intratumoral cystic changes, and peritumoral edema with increased echogenicity of the surrounding tissues [37].

Lipofibromatous Hamartoma

It is also called hamartoma of the nerve, fibrolipomatous nerve, neural fibrolipomatosis, and intraneural lipoma. This is characterized by the presence of fibrofatty infiltration around the nerve bundles. It may affect any nerve, but it has been more commonly reported in the wrist and hand, particularly in the median nerve. These cases can show digital enlargement due to increased perineural soft tissue and skin, which may cause macrodactylia [7, 38, 39].

On ultrasound, there is an enlargement of the nerve with hyperechoic tissue in between the neural fascicles. The neural bundles are more evident at higher frequencies and generate hypoechoic dots within the neural structure when scanning in a transverse view. In the presence of diffuse involvement of the soft-tissue nerves, there are multiple and tortuous hypoechoic tracts in the dermis and/or hypodermis. On color Doppler, this condition is usually hypovascular (Fig. 7.23) [7, 38].

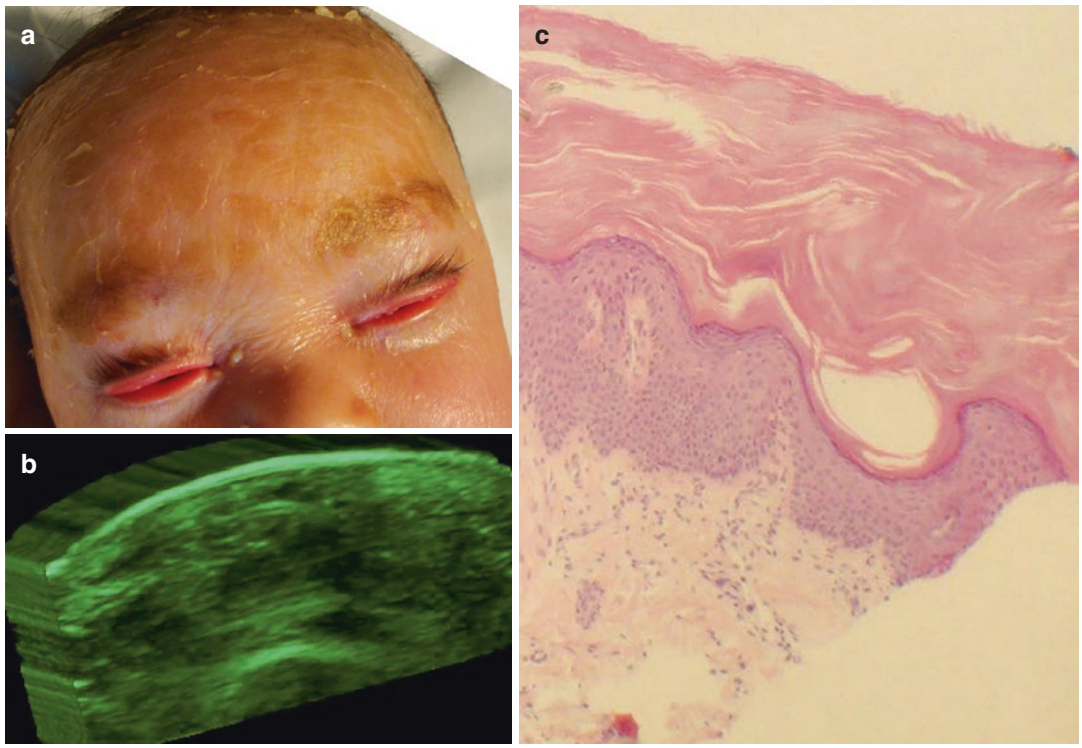

Fig. 7.23 Ichthyosis. (**a**) Clinical image. Notice the ectropion of the eyelids and the scaling of the skin. (**b**) 3D grayscale reconstruction shows epidermal thickening. (**c**) Histology (H&E 40×) presents epidermal thickening without signs of inflammation

Ichthyosis

Ichthyoses are a heterogeneous and rare group of cornification disorders characterized by generalized dry skin, scaling and hyperkeratosis, and erythroderma [40, 41].

A lamellar or congenital autosomal recessive ichthyosis is present at birth and implies a mutation in at least three loci of the chromosomes, which presents a normal life expectancy. However, there are other forms of presentations incompatible with life [7, 40, 41].

Clinically, the children are born with a membrane that appears as an extra layer of the skin with an erythrodermic base, also called a "collodion membrane." The skin shows a more rigid structure, which commonly causes other problems such as chronic eversion of the eyelids (ectropion) and lips (eclabion) [7, 40, 41].

Additionally, thickening of the skin of the palms and soles (palmoplantar keratoderma) and ungual dystrophies may be detected, among other changes. Sometimes, these alterations may be detected in prenatal scans [42].

On ultrasound, there is epidermal thickening and irregularities and diffuse thickening of the nail plates in all fingernails and toenails [7, 40, 41].

References

1. Boull C, Maguiness SM. Congenital hemangiomas. Semin Cutan Med Surg. 2016;35(3):124–7.
2. Braun V, Prey S, Gurioli C, et al. Congenital haemangiomas: a single-Centre retrospective review. BMJ Paediatr Open. 2020;4(1):e000816.
3. Nasseri E, Piram M, McCuaig CC, Kokta V, Dubois J, Powell J. Partially involuting congenital hemangiomas: a report of 8 cases and review of the literature. J Am Acad Dermatol. 2014;70(1):75–9.
4. ISSVA. ISSVA classification of vascular anomalies. https://www.issva.org/UserFiles/file/ISSVA-Classification-2018.pdf. Accessed 2018.
5. Gong X, Hua C, Xiong P, et al. Conventional ultrasonography and elastography for the diagnosis of congenital and infantile hemangiomas. J Dermatol. 2020;47(5):527–33.
6. Wortsman X. Atlas of dermatologic ultrasound. 1st ed. New York, NY: Springer International Publishing; 2018.
7. Wortsman X, Jemec GBE. Dermatologic ultrasound with clinical and histologic correlations. 1st ed. New York, NY: Springer-Verlag; 2013.
8. Rogers M, Lam A, Fischer G. Sonographic findings in a series of rapidly involuting congenital hemangiomas (RICH). Pediatr Dermatol. 2002;19(1):5–11.
9. Elluru RG. Cutaneous vascular lesions. Facial Plast Surg Clin North Am. 2013;21(1):111–26.
10. Rodríguez Bandera AI, Sebaratnam DF, Feito Rodríguez M, de Lucas LR. Cutaneous ultrasound and its utility in pediatric dermatology: part II-developmental anomalies and vascular lesions. Pediatr Dermatol. 2020;37(1):40–51.
11. Martinez-Lopez A, Salvador-Rodriguez L, Montero-Vilchez T, Molina-Leyva A, Tercedor-Sanchez J, Arias-Santiago S. Vascular malformations syndromes: an update. Curr Opin Pediatr. 2019;31(6):747–53.
12. John PR. Klippel-trenaunay syndrome. Tech Vasc Interv Radiol. 2019;22(4):100634.
13. Nishino K, Ito Y, Sorimachi T, Shimbo J, Fujii Y. Sturge-weber syndrome associated with arteriovenous malformation in a patient presenting with progressive brain edema and cyst formation. J Neurosurg Pediatr. 2010;5(5):529–34.
14. Ochoco G, Enriquez CAG, Urgel RJL, Catibog JS. Multimodality imaging approach in a patient with Klippel-Trenaunay syndrome. BMJ Case Rep. 2019;12(8):e228257.
15. Cherry KJ, Gloviczki P, Stanson AW. Persistent sciatic vein: diagnosis and treatment of a rare condition. J Vasc Surg. 1996;23(3):490–7.
16. Oduber CE, Young-Afat DA, van der Wal AC, van Steensel MA, Hennekam RC, van der Horst CM. The persistent embryonic vein in Klippel-Trenaunay syndrome. Vasc Med. 2013;18(4):185–91.
17. Ahuja AT, King AD, Metreweli C. Second branchial cleft cysts: variability of sonographic appearances in adult cases. AJNR Am J Neuroradiol. 2000;21(2):315–9.
18. Bagchi A, Hira P, Mittal K, Priyamvara A, Dey AK. Branchial cleft cysts: a pictorial review. Pol J Radiol. 2018;83:e204–9.
19. Bansal AG, Oudsema R, Masseaux JA, Rosenberg HK. US of pediatric superficial masses of the head and neck. Radiographics. 2018;38(4):1239–63.
20. Coste AH, Lofgren DH, Shermetaro C. Branchial cleft cyst. Treasure Island (FL): StatPearls. StatPearls Publishing Copyright © 2021, StatPearls Publishing LLC; 2021.
21. Hosokawa T, Takahashi H, Miyasaka Y, et al. Ultrasound evaluation of dermal sinuses/fistulas in pediatric patients. J Ultrasound Med. 2019;38(12):3107–22.
22. Ibrahim M, Hammoud K, Maheshwari M, Pandya A. Congenital cystic lesions of the head and neck. Neuroimaging Clin N Am. 2011;21(3).:621–639, viii.
23. Chang KV, Wu WT, Özçakar L. Thyroglossal duct cyst: dynamic ultrasound evaluation and sonoanatomy revisited. Med Ultrason. 2019;21(1):99–100.

24. Oyewumi M, Inarejos E, Greer ML, et al. Ultrasound to differentiate thyroglossal duct cysts and dermoid cysts in children. Laryngoscope. 2015;125(4):998–1003.
25. Patel S, Bhatt AA. Thyroglossal duct pathology and mimics. Insights Imaging. 2019;10(1):12.
26. Thompson LD. Thyroglossal duct cyst. Ear Nose Throat J. 2017;96(2):54–5.
27. Choi SJ, Choung YH, Park K, Bae J, Park HY. The variant type of preauricular sinus: postauricular sinus. Laryngoscope. 2007;117(10):1798–802.
28. Wortsman X, Jemec GB. Sonography of the ear pinna. J Ultrasound Med. 2008;27(5):761–70.
29. Patel DP, Castelo-Soccio L, Yan AC. Aplasia cutis congenita: evaluation of signs suggesting extracutaneous involvement. Pediatr Dermatol. 2018;35(1):e59–61.
30. Humphrey SR, Hu X, Adamson K, Schaus A, Jensen JN, Drolet B. A practical approach to the evaluation and treatment of an infant with aplasia cutis congenita. J Perinatol. 2018;38(2):110–7.
31. Happle R. Nevus sebaceus is a mosaic RASopathy. J Invest Dermatol. 2013;133(3):597–600.
32. Terenzi V, Indrizzi E, Buonaccorsi S, Leonardi A, Pellacchia V, Fini G. Nevus sebaceus of Jadassohn. J Craniofac Surg. 2006;17(6):1234–9.
33. Idriss MH, Elston DM. Secondary neoplasms associated with nevus sebaceus of Jadassohn: a study of 707 cases. J Am Acad Dermatol. 2014;70(2):332–7.
34. Wortsman X, Ferreira-Wortsman C, Corredoira Y. Ultrasound imaging of nevus sebaceous of Jadassohn. J Ultrasound Med. 2021;40(2):407–15.
35. Chen W, Jia JW, Wang JR. Soft tissue diffuse neurofibromas: sonographic findings. J Ultrasound Med. 2007;26(4):513–8.
36. Hung EH, Griffith JF, Ng AW, Lee RK, Lau DT, Leung JC. Ultrasound of musculoskeletal soft-tissue tumors superficial to the investing fascia. AJR Am J Roentgenol. 2014;202(6):W532–40.
37. James AW, Shurell E, Singh A, Dry SM, Eilber FC. Malignant peripheral nerve sheath tumor. Surg Oncol Clin N Am. 2016;25(4):789–802.
38. Boczar D, Forte AJ, Serrano LP, Trigg SD, Clendenen SR. Use of ultra-high-frequency ultrasound on diagnosis and management of Lipofibromatous Hamartoma: a technical report. Cureus. 2019;11(9):e5808.
39. Razzaghi A, Anastakis DJ. Lipofibromatous hamartoma: review of early diagnosis and treatment. Can J Surg. 2005;48(5):394–9.
40. Takeichi T, Akiyama M. Inherited ichthyosis: non-syndromic forms. J Dermatol. 2016;43(3):242–51.
41. DiGiovanna JJ, Robinson-Bostom L. Ichthyosis: etiology, diagnosis, and management. Am J Clin Dermatol. 2003;4(2):81–95.
42. Brandão P, Seco S, Loureiro T, Ramalho C. Prenatal sonographic diagnosis of harlequin ichthyosis. J Clin Ultrasound. 2019;47(4):228–31.